NASA Contractor Report 172576

ICASE REPORT NO. 85-24

NASA-CR-172576
19850018057

ICASE

FORCED MHD TURBULENCE IN A UNIFORM EXTERNAL MAGNETIC FIELD

Murshed Hossain
George Vahala
David Montgomery

Contract No. NAS1-17070
March 1985

INSTITUTE FOR COMPUTER APPLICATIONS IN SCIENCE AND ENGINEERING
NASA Langley Research Center, Hampton, Virginia 23665

Operated by the Universities Space Research Association

National Aeronautics and
Space Administration

Langley Research Center
Hampton, Virginia 23665

FORCED MHD TURBULENCE IN A UNIFORM EXTERNAL MAGNETIC FIELD

Murshed Hossain
Institute for Computer Applications in Science and Engineering

George Vahala
College of William and Mary
and
Institute for Computer Applications in Science and Engineering

David Montgomery
Dartmouth College

Abstract

Two-dimensional dissipative MHD turbulence is randomly driven at small spatial scales and is studied by numerical simulation in the presence of a strong uniform external magnetic field. A novel behavior is observed which is apparently distinct from the inverse cascade which prevails in the absence of an external magnetic field. The magnetic spectrum becomes dominated by the three longest-wavelength Alfvén waves in the system allowed by the boundary conditions: those which, in a box size of edge 2π, have wave numbers $(k_x, k_y) = (1, 0)$, $(1, 1)$, and $(1, -1)$, where the external magnetic field is in the x direction. At any given instant, one of these three modes dominates the vector potential spectrum, but they do not constitute a resonantly coupled triad. Rather, they are apparently coupled by the smaller-scale turbulence.

Research for the first and second author was supported by the National Aeronautics and Space Administration under NASA Contract No. NAS1-17070 while they were in residence at ICASE, NASA Langley Reserach Center, Hampton, VA 23665. Additional support for the second author was provided by the United States Department of Energy under Grant No. DE-FG05-84ER53176. The third author was supported by U.S.D.O.E. Grant No. DE-FG02-85ER53194 and NASA Grant No. NAG-W-710.

I. INTRODUCTION

A somewhat formalized problem in fluid and plasma turbulence which has received considerable attention in recent years is that of forced, dissipative turbulence which results when excitations are randomly injected into the medium at a well-defined length scale. The three-dimensional Kolmogoroff direct cascade which results in fluid turbulence[1] is familiar, as are (by now) the "inverse" cascades which result in two-dimensional fluid flows[2-5] and in two-[6-8] and three-dimensional magnetofluids.[9-13]

Most of the effort so far has been expended on isotropic media and the similarity-variable power-law spectra which can be predicted by Kolmogoroff-style dimensional analysis. Particularly in the case of a plasma in the presence of a strong external magnetic field, the assumption of isotropy is not a good one, for the magnetic field renders even an initially isotropic spectrum strongly anisotropic, as recently demonstrated by Shebalin, et al.[14]

Here, we report a numerical study of forced two-dimensional MHD turbulence in the presence of an externally-imposed uniform magnetic field. Hossain[15] et al., have previously studied the long-time evolution of an inverse cascade of magnetic vector potential for this system. Here, we are interested in the possibility that the external magnetic field may suppress or modify the inverse cascade.

In the presence of the uniform external magnetic field, the usual arguments[13] used to suggest the possibility of inverse cascades no longer apply. The ideal magnetic invariant (mean square vector potential) is no longer one that survives truncation in Fourier space. The absolute equilibrium Gibbs ensemble no longer predicts condensation at the longest allowed wavelength in the limit of an infinite number of degrees of freedom.

There is no longer any a priori reason to expect an inverse cascade or any enhanced transfer to long wavelengths in the spectrum of any particular quantity.

Somewhat to our surprise, we have found that a substantial amount of long-wavelength excitation results from injection at a short-wavelength forcing band. The magnetic spectrum becomes dominated, in a rather unfamiliar way, by the three longest-wavelength Alfvén waves allowed by the boundary conditions. The back-transfer ceases before these three Fourier coefficients contain the same high fraction (> 90%) of the total mean square vector potential as the two longest wavelengths did with no external magnetic field, but they still come to dominate the spectrum. The resulting state does not fit neatly into the developed taxonomy of inverse cascades[13] for the isotropic case, and we are uncertain as to what to call the new phenomenon.

In Section II we set out the dynamical equations and numerical procedure. The computed results are reported in Section III. Section IV is given over to discussion and comparison with a relevant hydrodynamic[16] parallel, that of Rossby waves.

II. DYNAMICAL EQUATIONS AND NUMERICAL PROCEDURE

We use the equations of incompressible MHD in what has by now become a familiar dimensionless form:

$$\frac{\partial \underset{\sim}{v}}{\partial t} = -\underset{\sim}{v}\cdot\nabla\underset{\sim}{v} + \underset{\sim}{j} \times \underset{\sim}{B} - \nabla p + \frac{1}{R}\nabla^2 \underset{\sim}{v} \tag{1}$$

$$\frac{\partial \underset{\sim}{B}}{\partial t} = \nabla \times (\underset{\sim}{v} \times \underset{\sim}{B}) + \frac{1}{R_M}\nabla^2 \underset{\sim}{B}, \tag{2}$$

where $\underset{\sim}{B}$ is the magnetic field, $\underset{\sim}{v}$ is the velocity field, $\underset{\sim}{j}$ is the current density, p is the pressure, and $\nabla\cdot\underset{\sim}{v} = 0 = \nabla\cdot\underset{\sim}{B}$. Moreover, $\underset{\sim}{j} = \nabla \times \underset{\sim}{B}$. The pressure p is determined by taking the divergence of Eq. (1). R and R_M are the mechanical and magnetic Reynolds numbers, respectively:

$$R = U_0 L_0/\nu, \quad R_M = L_0 U_0/\eta \tag{3}$$

where L_0 is a length scale, U_0 is a typical flow speed, and ν and η are the kinematic viscosity and magnetic diffusivity, respectively.

We will treat the two-dimensional case, in a limit in which $\partial/\partial z \equiv 0$ for all field variables. $\underset{\sim}{B}$ and $\underset{\sim}{v}$ are assumed to have only x and y components, and to obey periodic boundary conditions over a square box of edge 2π. $\underset{\sim}{B}$ will be divided into a uniform part $\underset{\sim}{B}_0 = B_0 \hat{e}_x$ and a fluctuating part with zero spatial average $\underset{\sim}{B}_f$, so that $\underset{\sim}{B} = B_0 \hat{e}_x + \underset{\sim}{B}_f$. The vector potential $a_f \hat{e}_z$, assumed spatially periodic, will be used to represent

$$\underset{\sim}{B}_f = \nabla \times \hat{e}_z a_f. \tag{4}$$

Notice that the total vector potential, $\underset{\sim}{a} = (a_f + yB_0)\hat{e}_z$, is <u>not</u> spatially periodic, even though $\underset{\sim}{B}$ is.

The velocity field $\underset{\sim}{v}$ will be derived from a stream function ψ, so that $\underset{\sim}{v} = \nabla\psi \times \hat{e}_z$. The vorticity $\omega = -\nabla^2 \psi$, and the current $j = -\nabla^2 a_f$.

Taking a curl of Eq. (1) and removing a curl from Eq. (2), we have the dynamical equations in a familiar and computationally useful form:

$$\frac{\partial \omega}{\partial t} = -\underset{\sim}{v}\cdot\nabla\omega + \underset{\sim}{B}_f\cdot\nabla j + \nu_* \nabla^2 \omega + B_0 \frac{\partial j}{\partial x} + F \tag{5}$$

$$\frac{\partial a_f}{\partial t} = -\underset{\sim}{v}\cdot\nabla a_f + \eta_* \nabla^2 a_f + B_0 \frac{\partial \psi}{\partial x} + G. \tag{6}$$

In Eqs. (5) and (6), $\nabla \times \underset{\sim}{B} = j\hat{e}_z$, and $\nu_* = R^{-1}$, $\eta_* = R_M^{-1}$. We have added random forcing functions $F = F(x, y, t)$ and $G = G(x, y, t)$, which are understood as an arbitrary external source of random excitations at the small scales whose statistics will be specified later. They are understood to represent a variety of possible sources of turbulence.

All variables are represented as complex Fourier series, e.g.,

$$\begin{aligned} a_f &= \sum_{\underset{\sim}{k}} a(\underset{\sim}{k}, t)\exp(i\underset{\sim}{k}\cdot\underset{\sim}{x}) \\ \omega &= \sum_{\underset{\sim}{k}} \omega(\underset{\sim}{k}, t)\exp(i\underset{\sim}{k}\cdot\underset{\sim}{x}), \end{aligned} \tag{7}$$

where the allowed wave-vectors $\underset{\sim}{k} = (k_x, k_y)$ can have only integer components, not both zero. By reality of ω, for example, $\omega(-\underset{\sim}{k}) = \omega^*(\underset{\sim}{k})$, always.

For computational purposes, k_x and k_y are limited to the range $-N/2 + 1$ to $N/2$, where the integer N is two raised to some appropriate power. Isotropic truncation in $\underset{\sim}{k}$-space is implemented in order to take advantage of the Orszag-Patterson[17] transform methods, which we employ throughout.

The forcing functions in Fourier space, $F(\underset{\sim}{k}, t)$ and $G(\underset{\sim}{k}, t)$, are chosen to be non-zero only inside a certain "forcing band," $k_{min} \leq |\underset{\sim}{k}| \leq k_{max}$.[5,8,15,18,19] For wave numbers inside the forcing band, the forcing functions are advanced from the nth to the (n + 1)st time step (except for Run E) according to the prescription

$$F^{n+1}(\underset{\sim}{k}) = fF^{n}(\underset{\sim}{k}) + \sqrt{1 - f^2}\, J^{n+1}(\underset{\sim}{k}). \tag{8a}$$

f is a memory factor, usually set equal to 0.95, while J is generated from a Gaussian random number generator. For Run E we have used a constant amplitude random phase algorithm with no memory, viz.,

$$F^{n}(\underset{\sim}{k}) = c \exp(i\phi), \tag{8b}$$

where the random phase angle ϕ lies between $-\pi$ and π.

Eqs. (5) and (6) have been solved as an initial value problem, starting with all empty spectra (except for Run H), for the parameters listed in Table 1. Our comments in Section III are limited to a subset of these runs. The forcing bands were typically $55 \leq k^2 \leq 70$ with a few exceptions of $95 \leq k^2 \leq 110$ (Table 1). F and G are assumed to be uncorrelated. The time step is $\Delta t = (256)^{-1}$.

III. NUMERICAL RESULTS

The time development of the mean square vector potential $A(t) \equiv \sum_{\underset{\sim}{k}} |a_f(\underset{\sim}{k}, t)|^2$, is shown in Fig. 1a for two cases: no external magnetic field (Run A, with $B_0 = 0$) and with an external field (Run C, with $B_0 = .5$). The same forcing functions were employed in both cases.

In Run A ($B_0 = 0$), we see that A(t) continues to increase systematically over about 200 units of time, while for Run C ($B_0 = .5$), a limiting value is reached in considerably less time than that. (One unit of time is an Alfvén transit time of unit distance in a unit magnetic field.)

Our earlier computations indicate that in the $B_0 = 0$ case, A(t) will also eventually reach a saturated value, in which the rate of supply from the smaller scales to the largest scales will be balanced, for the longest wavelengths, by their own dissipation. If that is the case for Run C, then it follows that a vastly reduced rate of supply of A(t) from the smaller scales is present.

The behavior of A(t) for Run C is similar to the behavior of the total energy E(t),

$$E(t) = \sum_{\underset{\sim}{k}} \left[|\underset{\sim}{v}(\underset{\sim}{k}, t)|^2 + |\underset{\sim}{B}(\underset{\sim}{k}, t)|^2 \right] \tag{9}$$

for the $B_0 = 0$ case, as is shown in Fig. 1b. This is more like the bahavior to be expected from a directly-cascaded quantity.

Figs. 2a, 2b show the mean-square fluctuating vector potential and energy, respectively, for Run B, with $B_0 = 1$. The same variables for Run C ($B_0 = .5$) are displayed on an expanded scale in Figs. 3a, 3b. The large fluctuations in A(t) are a reflection of the domination of the $\underset{\sim}{k}$ spectrum by the three longest-wavelength Alfvén waves, those with $\underset{\sim}{k}$ vectors equal to $(k_x, k_y) = (1, 0)$, $(1, 1)$, and $(1, -1)$. We find (as is typical for Alfvén waves) that for each of these modes the energy, averaged over a period, is shared equally between the velocity field and the magnetic field. (The fields oscillate 180^o out of phase with each other.)

Fig. 4a is a set of contours of constant a_f for Run A ($B_0 = 0$) at time $t = 234.37$ (time step 60,000). The dashed contours indicate negative values. The characteristic grouping of regions of positive and negative a_f is apparent. Similar contour plots for Run B appear in Fig. 4b. A reduced, but still significant, grouping of like-signed regions of a_f is visible.

The quasi-periodic behavior of the mean square vector potential may be displayed by considering the Fourier decomposition of the bulk quantity $A(t)$:

$$A(\omega_n) = \frac{1}{N} \sum_{m=0}^{N-1} A(t_m) \exp(-i\omega_n t_m). \tag{10}$$

Individual modal squared vector potentials may be similarly defined as

$$A(\underset{\sim}{k}, \omega_n) = \frac{1}{N} \sum_{m=0}^{N-1} |a_f(\underset{\sim}{k}, t_m)|^2 \exp(-i\omega_n t_m), \tag{11}$$

and in Eqs. (10) and (11), $t_m \equiv m\Delta t$, $\omega_n \equiv 2\pi n/T$, with $n = -\frac{N}{2} + 1$, $-N/2 + 2, \cdots, N/2$, and T is the total duration of the time interval over which the Fourier decomposition is to be carried out. The spectra so defined are computed for Runs A through D and are displayed in Figs. 5a to 5d, respectively. For all cases with $B_0 \neq 0$, the spectra exhibit a pronounced peak around the Alfvén frequency $\omega = 2\underset{\sim}{k}\cdot\underset{\sim}{B}_0 = 2k_x B_0$, which is just $2B_0$ for $k_x = 1$. The factor of two is an artifice of the fact that we are considering <u>squares</u> of amplitudes rather than amplitudes. It should be noted that we have suppressed the zero frequency peak in the spectrum, which corresponds to the non-zero mean value of $A(t)$, and we have plotted only up to a cutoff frequency ω_{max} (typically, $\omega_{max} = 8$), above which the spectra are very low. It is interesting that this qualitative behavior of the spectrum, with its sharp peak at the Alfvén frequency, is independent of the magnitudes of viscosity and magnetic diffusivity.

Upon time averaging, it is found that the three modes (1, 0), (1, 1), and (1, -1) contain about 35% of the total mean square vector potential. This is a large fraction, but smaller than the very large fraction (> 90%)

eventually accounted for by the (1, 0) and (0, 1) modes in the $B_0 = 0$ cases.

Figs. 6a, 6b, 6c show the power spectra for just the three modal vector potentials associated with $(k_x, k_y) = (1, 0)$, (1, 1), and (1, -1). It is of interest to note that these three modes do not pass excitations to each other directly, since they do not constitute a resonantly coupled triad, but are only indirectly coupled by the other, lower-amplitude turbulent coefficients. Fig. 7 shows the relative contribution of these modes to the total A.

A mean magnetic wave number may be defined by $k^2_{mean} = E_B/A$, where E_B is the magnetic term in Eq. (9). For $B_0 = 0$, this ratio has been observed to approach $k_{min} = 1$ as t increases. For example, in Run A, k_{mean} has become about 2.4 by $t = 120$, and continues to decrease. For $B_0 = 1$, k_{mean} approaches about 5.5 and fluctuates unsystematically about that value. In both cases, a typical number for the injection would be $k = 8$, which is the approximate center of the forcing band $55 \leq k^2 \leq 70$.

It is also of interest to assess the degree of anisotropy which may result from the isotropic forcing function. Following Shebalin, et al.,[14] we may introduce the anisotropy angle θ_Q for any field Q as

$$\theta_Q = \tan^{-1}\left\{ \sum_{\underset{\sim}{k}} k_\perp^2 \, |Q(\underset{\sim}{k}, t)|^2 / \sum_{\underset{\sim}{k}} k_\parallel^2 \, |Q(\underset{\sim}{k}, t)|^2 \right\} . \qquad (12)$$

Q can be any of the fields a_f, $\underset{\sim}{B}$, $\underset{\sim}{v}$, j, ψ, or ω. For an isotropic spectrum, θ_Q will be 45^o. In Figs. 8a to 8f, the anisotropy angles are shown for each of the six field variables for the case of Run B ($B_0 = 1.0$). In all cases, the anisotropy is seen to rise rapidly, in the same direction as

observed by Shebalin, et al., and then to decay slightly and to fluctuate. The higher anisotropy in the more differentiated quantities j and ω, which emphasize the high-$\underset{\sim}{k}$ parts of the spectrum, and which were observed by Shebalin, et al., are not found here. The major contributions to the anisotropy here come more from the low-$\underset{\sim}{k}$ modes than in the Shebalin computations.

The adequacy of the spatial resolution used in these computations should be remarked upon, for it was not as good as one would have liked. Typically, the computed Kolmogoroff dissipation wave number was three or four times k_{max}. It would be of interest to re-do these computations at much higher resolution (say, 128 × 128) for the same dissipation coefficients and forcing functions.

IV. DISCUSSION

The initial results from solving the two-dimensional, incompressible equations of MHD turbulence in the presence of random, small-scale, mechanical and magnetic forcing are that a state develops in which the magnetic spectrum is dominated by only three modes. These modes, which do not constitute a resonantly coupled triad, are the three longest-wavelength Alfvén waves allowed by the periodic boundary conditions: $(k_x, k_y) = (1, 0)$, $(1, 1)$, and $(1, -1)$. [The mode $(0, 1)$ is not an Alfvén wave, since $\omega = \underset{\sim}{k}\cdot\underset{\sim}{B}_0 = 0$, in the present geometry.] The three modes are coupled only through the smaller-scale turbulence.

For a given forcing function, the level of excitations for both magnetic potential and energy is substantially lower with the external magnetic field than without it. This can be due to (1) the suppression of the inverse

cascade to a considerable extent since the usual predictors of inverse cascade behavior are absent for a finite B_0; or (2) a reduced rate of supply of the cascadable rugged invariants (the supply rate is not determined by the forcing function alone); or (3) a combination of (1) and (2). The domination of the magnetic spectrum by the three long-wavelength Alfvén waves is a striking phenomenon, and one that deserves further study. Of particular interest is whether the phenomenon will persist in three dimensions.

An imperfect parallel situation exists in the case of Rossby waves in two-dimensional Navier-Stokes turbulence, as investigated by Rhines.[16,20,21] There also, the linearized wave equations exhibit wave propagation with a frequency having a highly anisotropic dependence upon angle. A significant difference in the two situations is that the frequencies of the linearized waves go to zero as $k \to \infty$ for <u>all</u> angles, so that the wave-like properties disappear at small scales, for the Rossby-wave case. Down to some wave number, the fluid behaves in an essentially Navier-Stokes way. Rhines found an "incomplete" inverse cascade, in the sense that in the wave number range in which the oscillatory properties were negligible, the back-transfer seemed to be unimpaired; however, the transfer became inhibited at the longer wavelengths and while macroscopic vortices did become apparent, they were smaller than the box size. Our situation does not have the feature that the frequency of the linear waves goes to zero at very short wavelengths, and significant differences from Rhines's spectrum were observed.

In summary, the non-resonant three-mode behavior displayed here is an interesting phenomenon and deserves further study. We are unaware of anything quite like it in turbulent systems previously studied. Greater spatial resolution and higher Reynolds numbers seem likely to exhibit the phenomenon in cleaner form.

REFERENCES

[1]G. K. Batchelor, Homogeneous Turbulence (Cambridge, U.K.; Cambridge University Press, 1953).

[2]R. H. Kraichnan, Phys. Fluids 10, 1417 (1967).

[3]C. E. Leith, Phys. Fluids 11, 671 (1968).

[4]G. K. Batchelor, Phys. Fluids 12, Suppl. II, 233 (1969).

[5]D. K. Lilly, Phys. Fluids 12, Suppl. II, 240 (1969).

[6]D. Fyfe and D. Montgomery, J. Plasma Phys. 16, 181 (1976).

[7]D. Fyfe, G. Joyce, and D. Montgomery, J. Plasma Phys. 17, 317 (1977).

[8]D. Fyfe, D. Montgomery, and G. Joyce, J. Plasma Phys. 17, 369 (1977).

[9]U. Frisch, A. Pouquet, J. Leorat, and A. Mazure, J. Fluid Mech. 68, 769 (1975).

[10]A. Pouquet, U. Frisch, and J. Leorat, J. Fluid Mech. 77, 321 (1976).

[11]M. Meneguzzi, U. Frisch, and A. Pouquet, Phys. Rev. Lett. 47, 1060 (1981).

[12]D. Mongtomery, Phys. Scripta T2:1, 83 (1982).

[13]R. H. Kraichnan and D. Montgomery, Rep. Progr. Phys. 43, 547 (1980).

[14]J. V. Shebalin, W. H. Matthaeus, and D. Montgomery, J. Plasma Phys. 29, 525 (1983).

[15]M. Hossain, W. H. Matthaeus, and D. Montgomery, J. Plasma Phys. 30, 479 (1983).

[16]P. B. Rhines, J. Fluid Mech. 69, 417 (1975).

[17]S. A. Orszag, Stud. Appl. Math. 50, 293 (1971); G. S. Patterson and S. A. Orszag, Phys. Fluid 14, 2538 (1971).

[18]U. Frisch and P. L. Sulem, Phys. Fluids 27, 1921 (1984).

[19]U. Frisch and P. L. Sulem, Phys. Fluids 28, 438 (1985).

[20]G. Holloway and M. C. Hendershott, J. Fluid Mech. 82, 747 (1977).

[21]A. Hasegawa, "Self-Organization Process in Continuous Media," Bell Labs. preprint (Murray Hill, New Jersey, 1985); to be published.

Table 1

Run	(N × N) Grid	B_0	ν_*, η_*	Mean Forcing Wave Number	Initial Spectrum	Forcing Algorithm
Run A	32 × 32	0.0	.002	8	empty	Gaussian
Run B	32 × 32	1.0	.002	8	empty	Gaussian
Run C	32 × 32	0.5	.002	8	empty	Gaussain
Run D	32 × 32	2.0	.002	8	empty	Gaussian
Run E	32 × 32	1.0	.002	8	empty	Flat
Run F	32 × 32	0.5	.002	10	empty	Gaussian
Run G	64 × 64	0.5	.002	10	empty	Gaussian
Run H	64 × 64	1.0	.002	10	isotropic	Gaussian
Run I	32 × 32	1.0	.001	8	empty	Gaussian

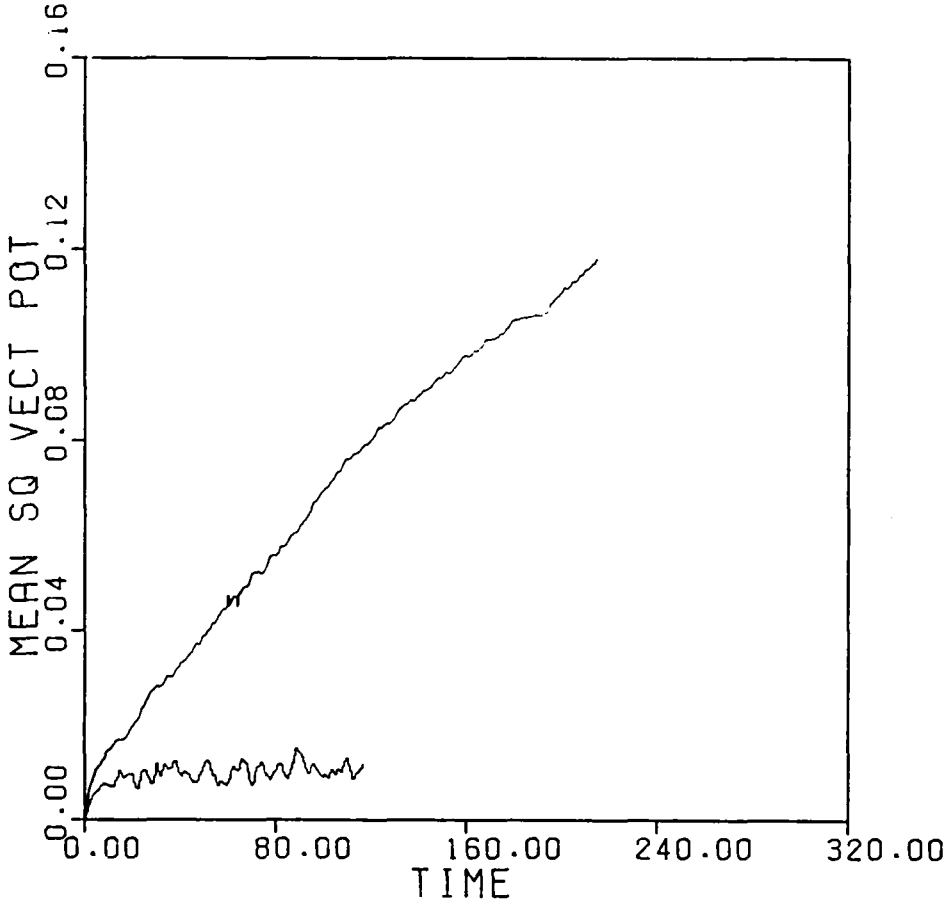
MEAN SQ VECT POT
0.00
0.04
0.08
0.12
0.16
0.00
80.00
160.00
240.00
320.00
TIME

Fig. 1(a)

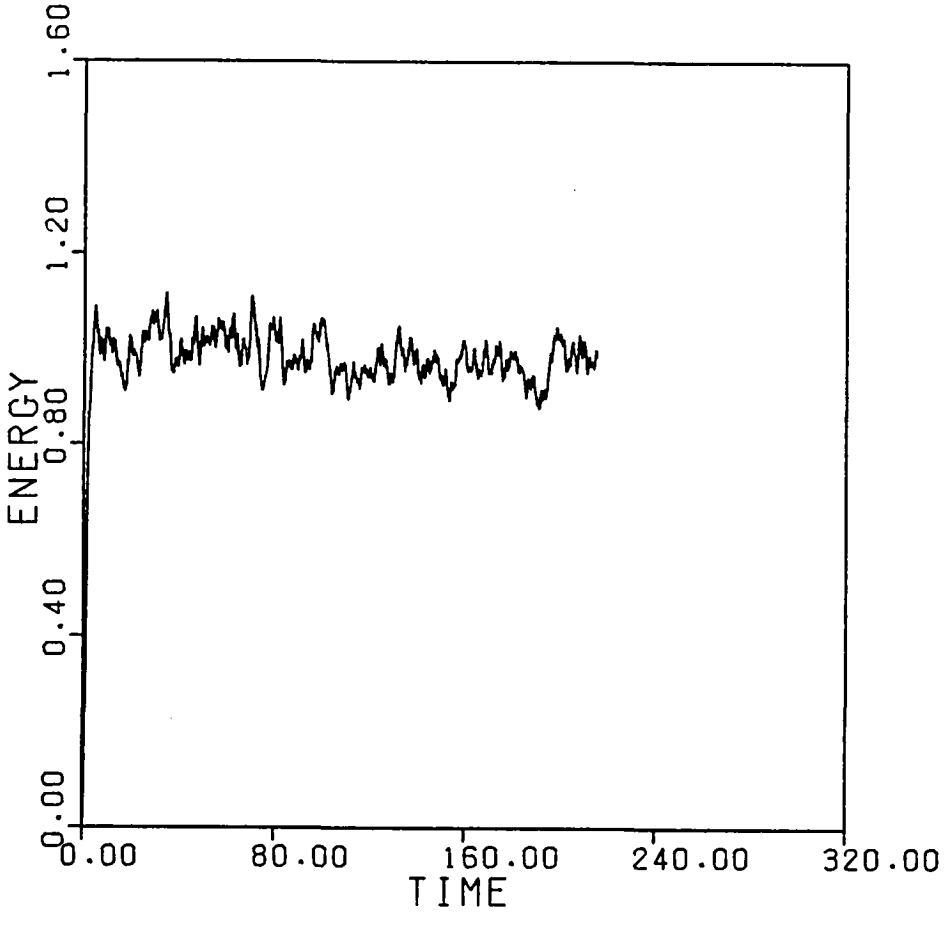

Fig. 1(b)

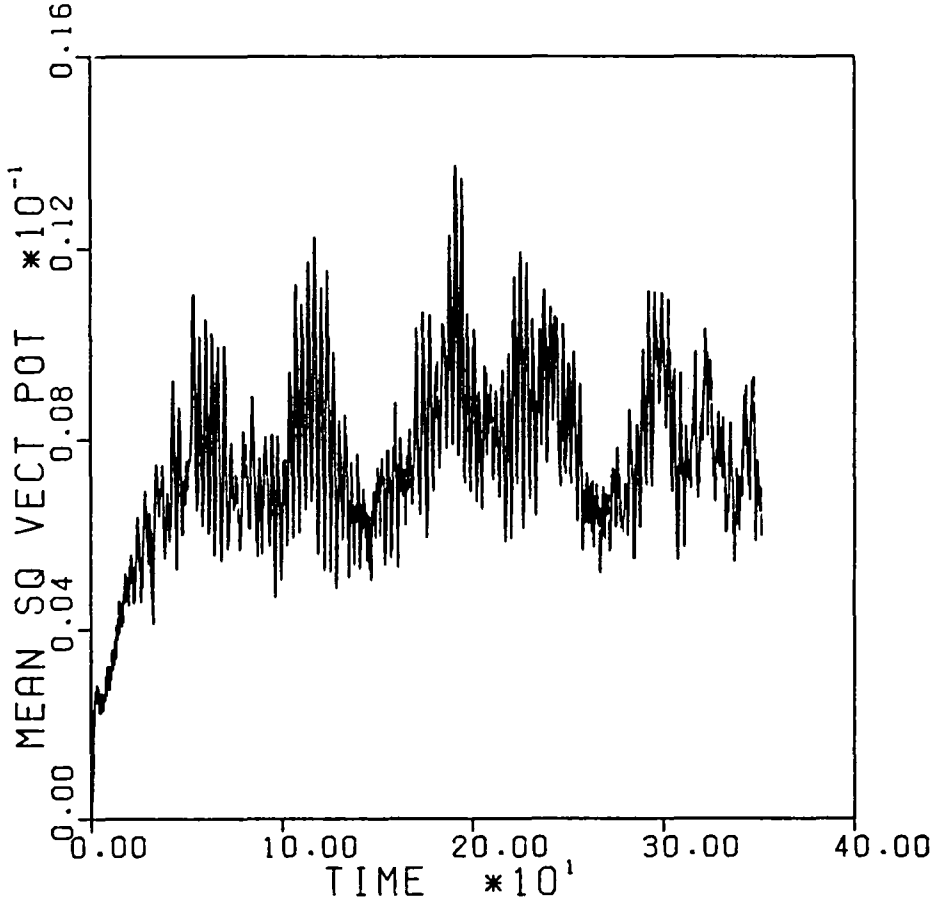
MEAN SQ VECT POT *10⁻¹
0.00
0.04
0.08
0.12
0.16
0.00
10.00
20.00
30.00
40.00
TIME *10¹

Fig. 2(a)

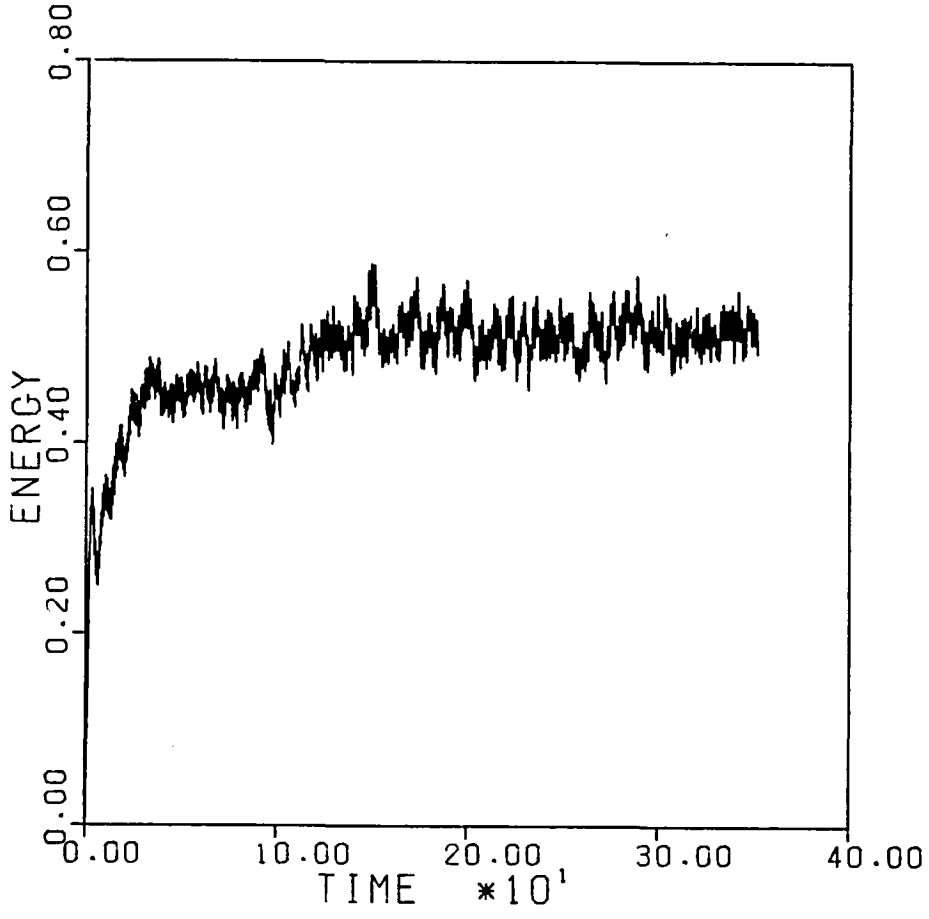

Fig. 2(b)

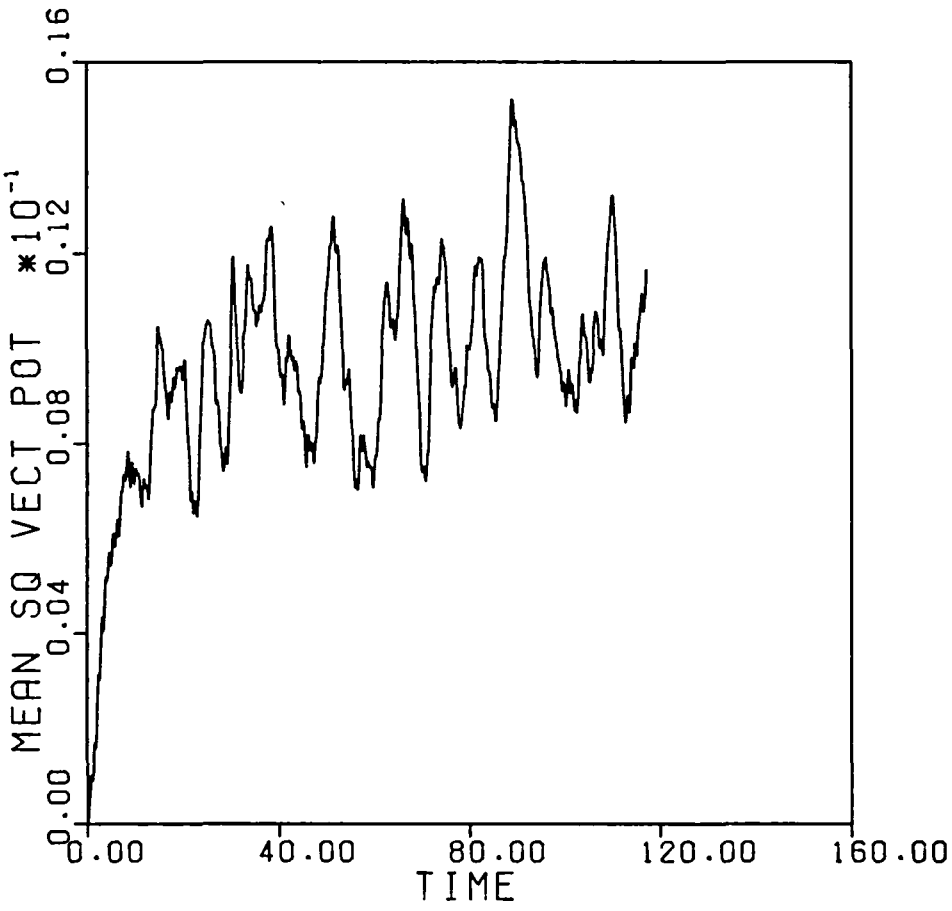
MEAN SQ VECT POT *10⁻¹
0.00
0.04
0.08
0.12
0.16
0.00
40.00
80.00
120.00
160.00
TIME

Fig. 3(a)

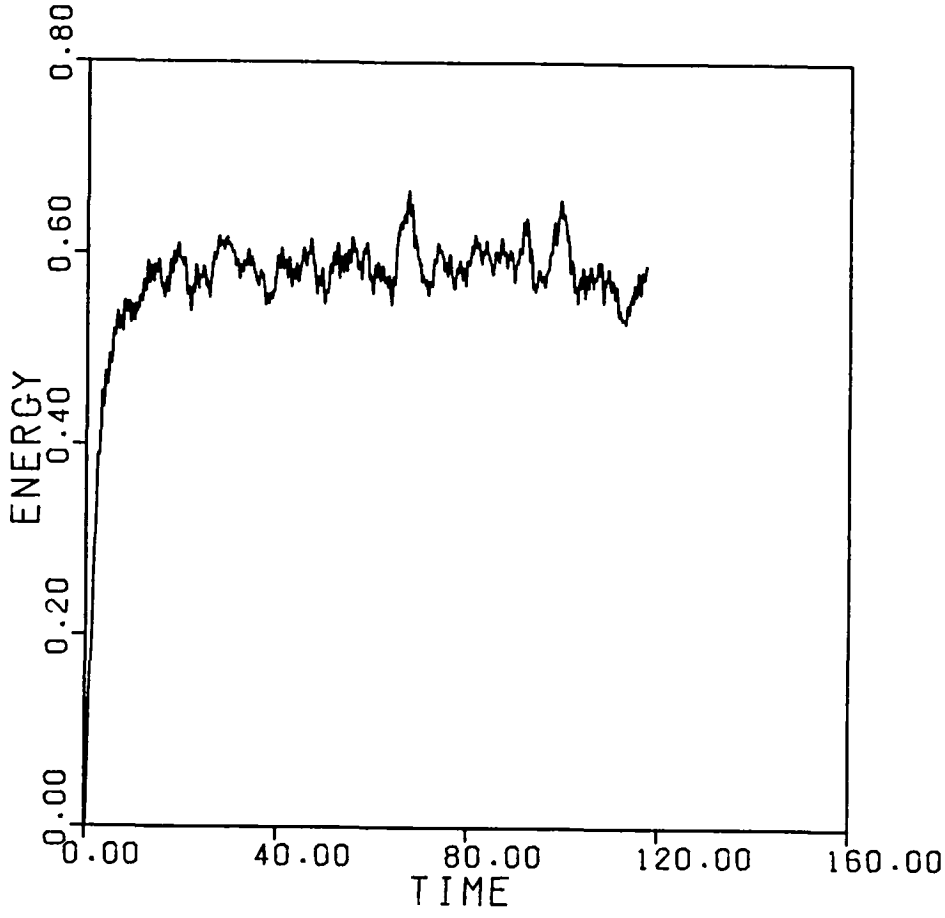

Fig. 3(b)

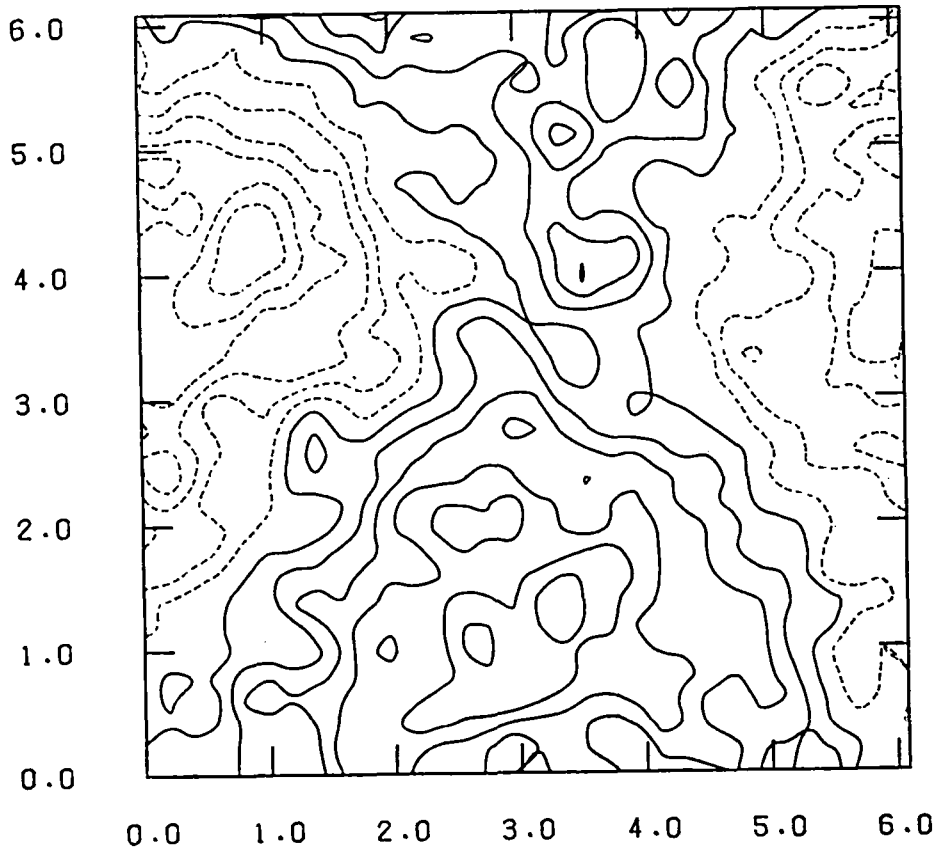

Fig. 4(a)

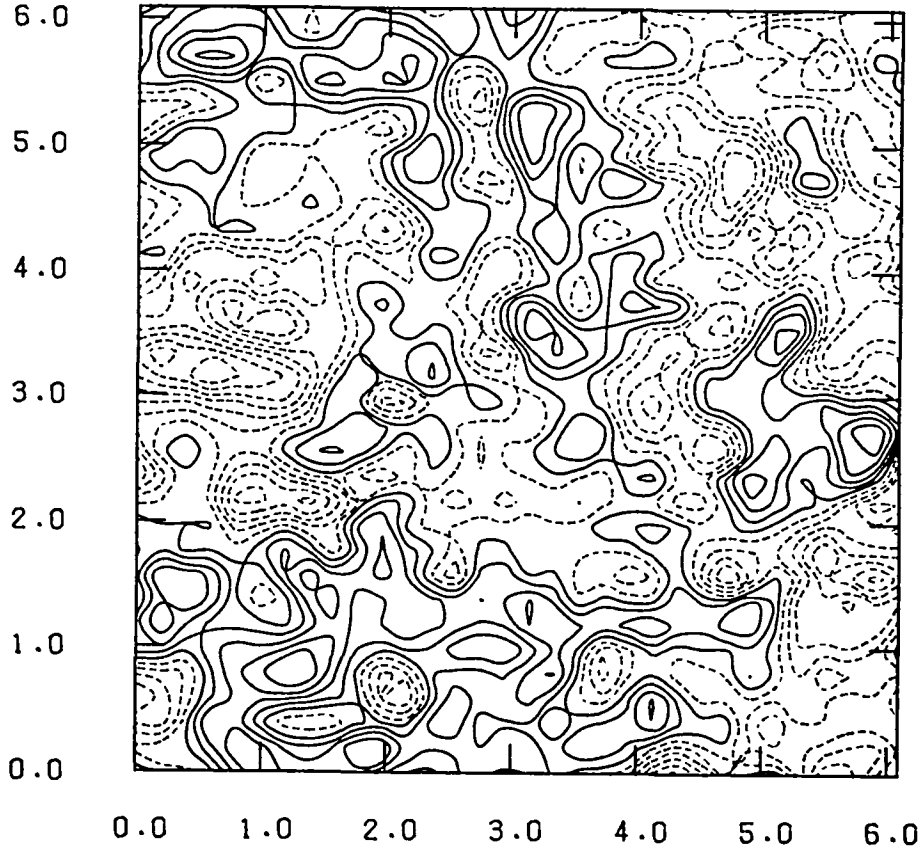

Fig. 4(b)

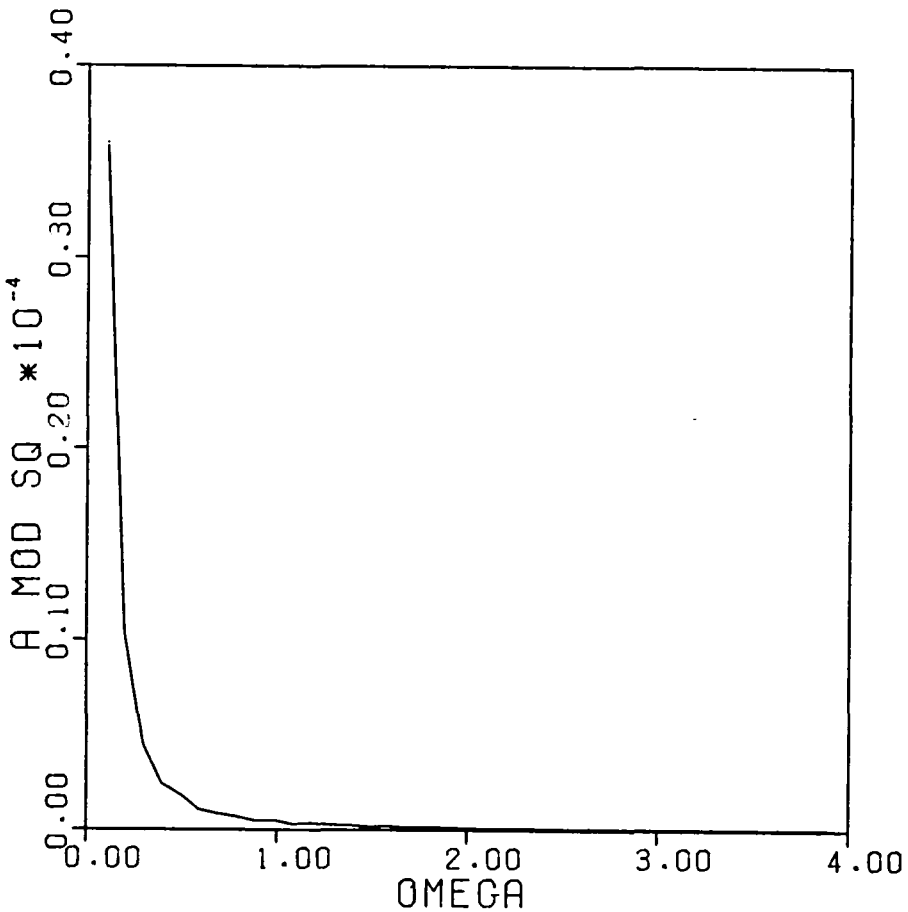

Fig. 5(a)

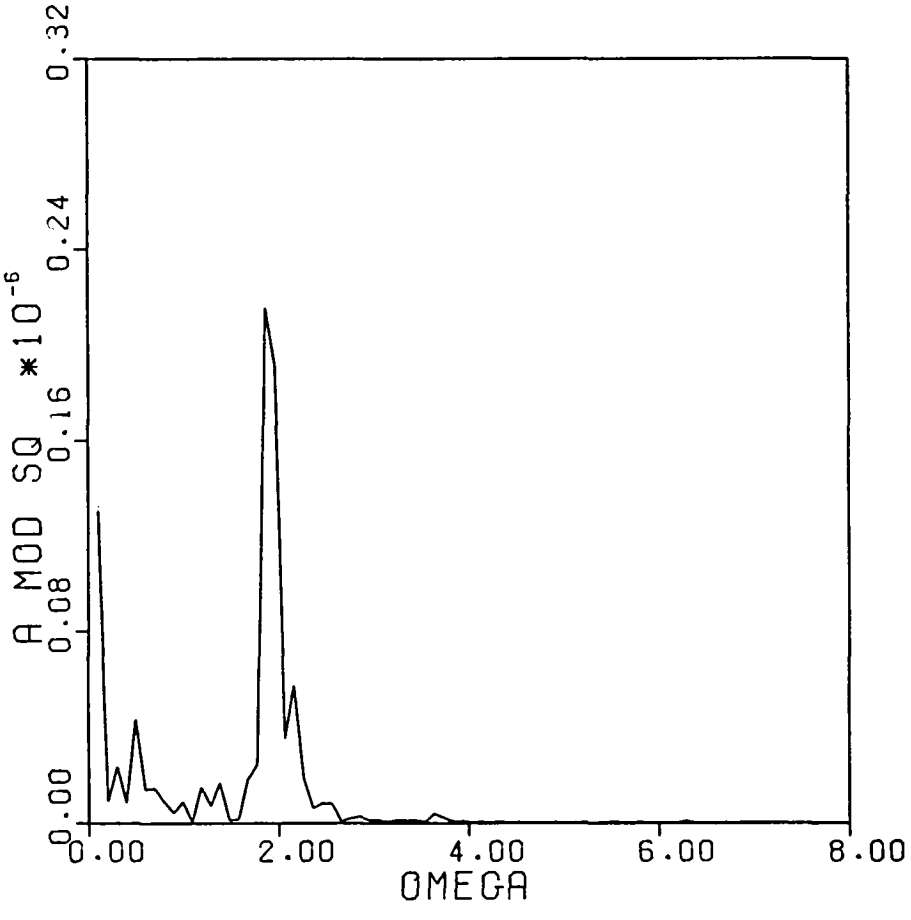

Fig. 5(b)

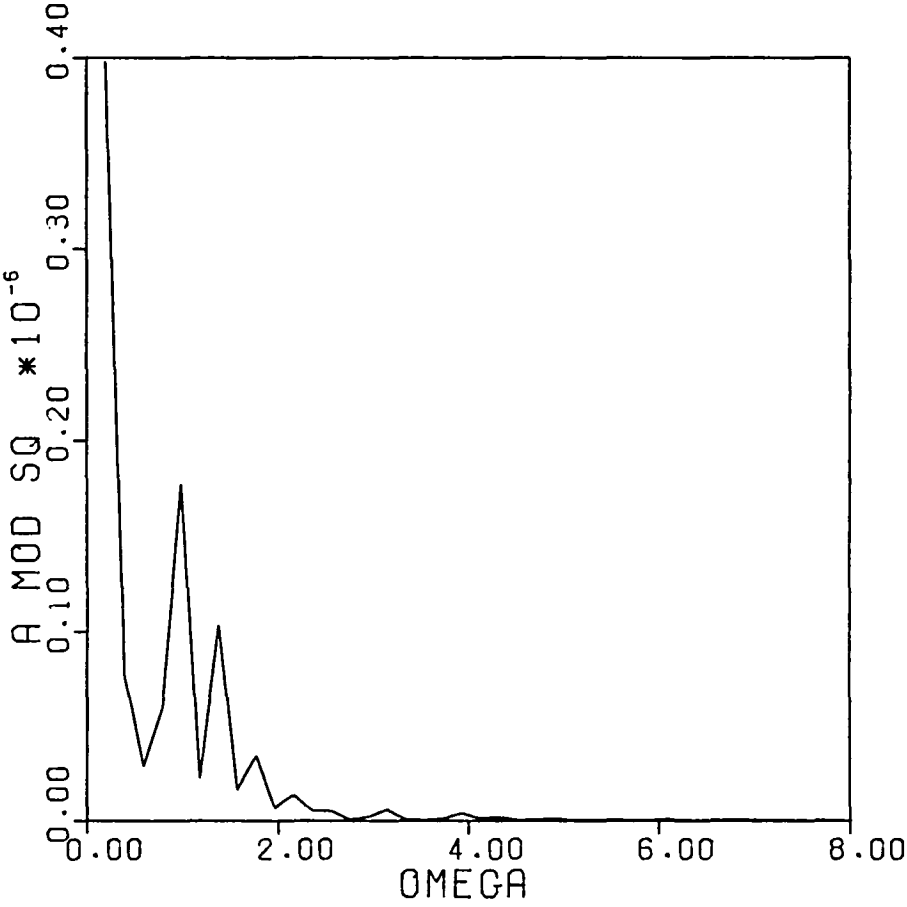

Fig. 5(c)

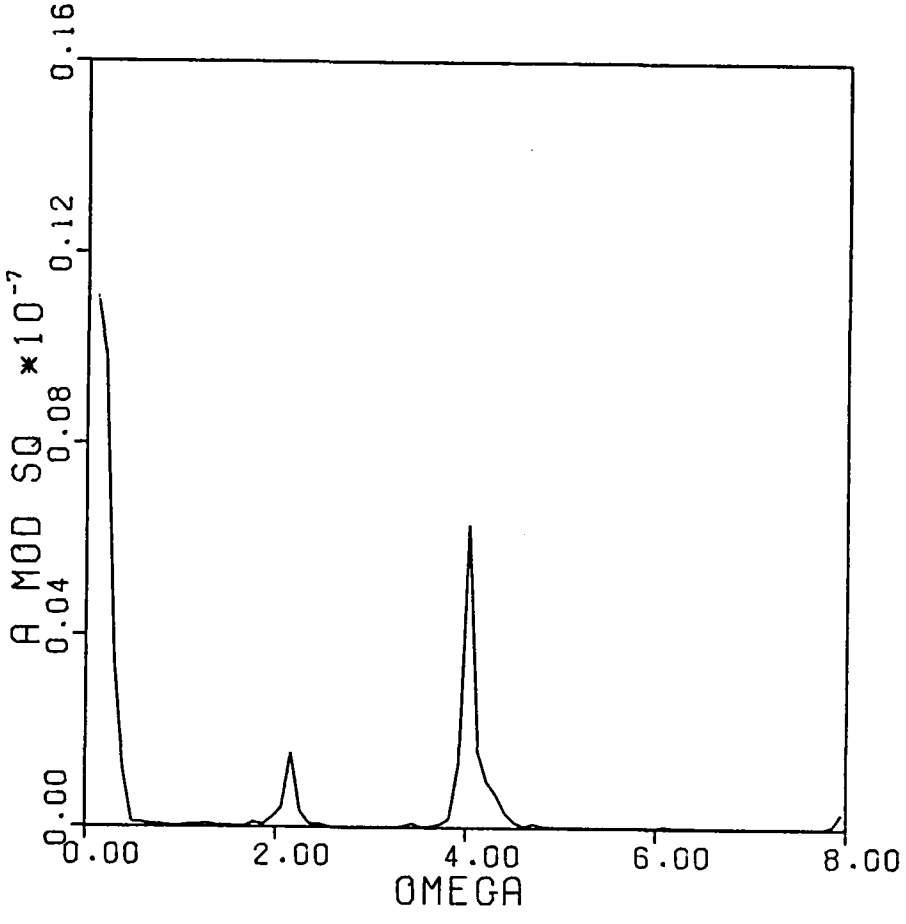

Fig. 5(d)

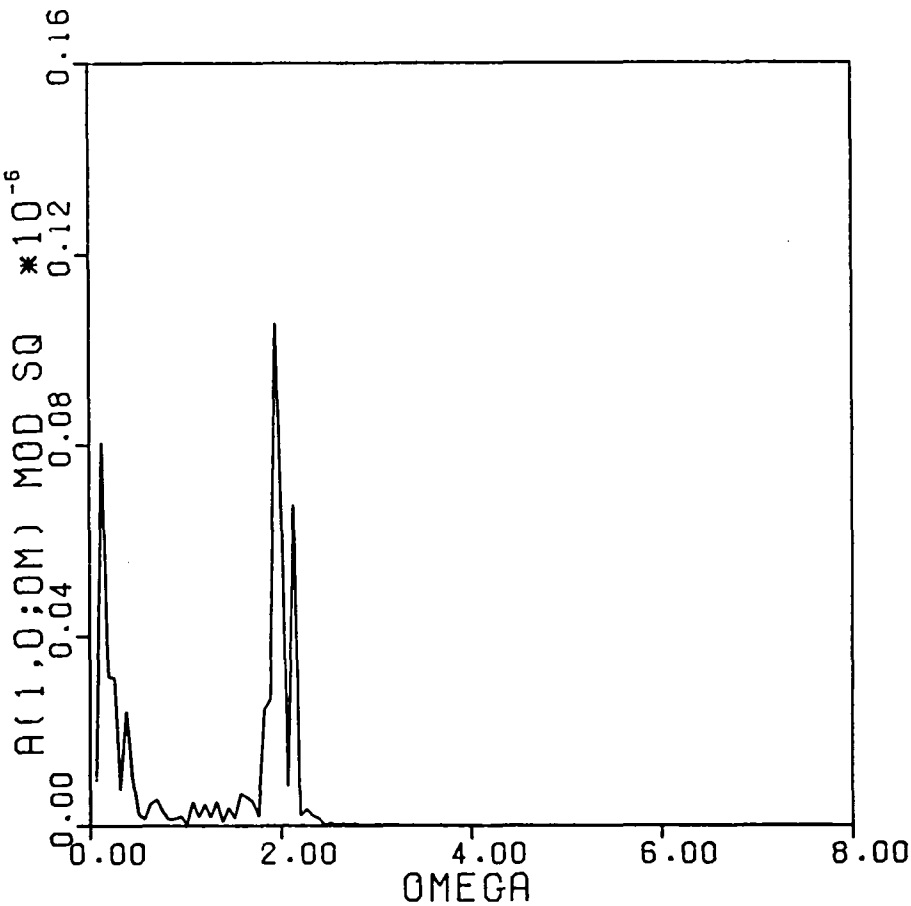

Fig. 6(a)

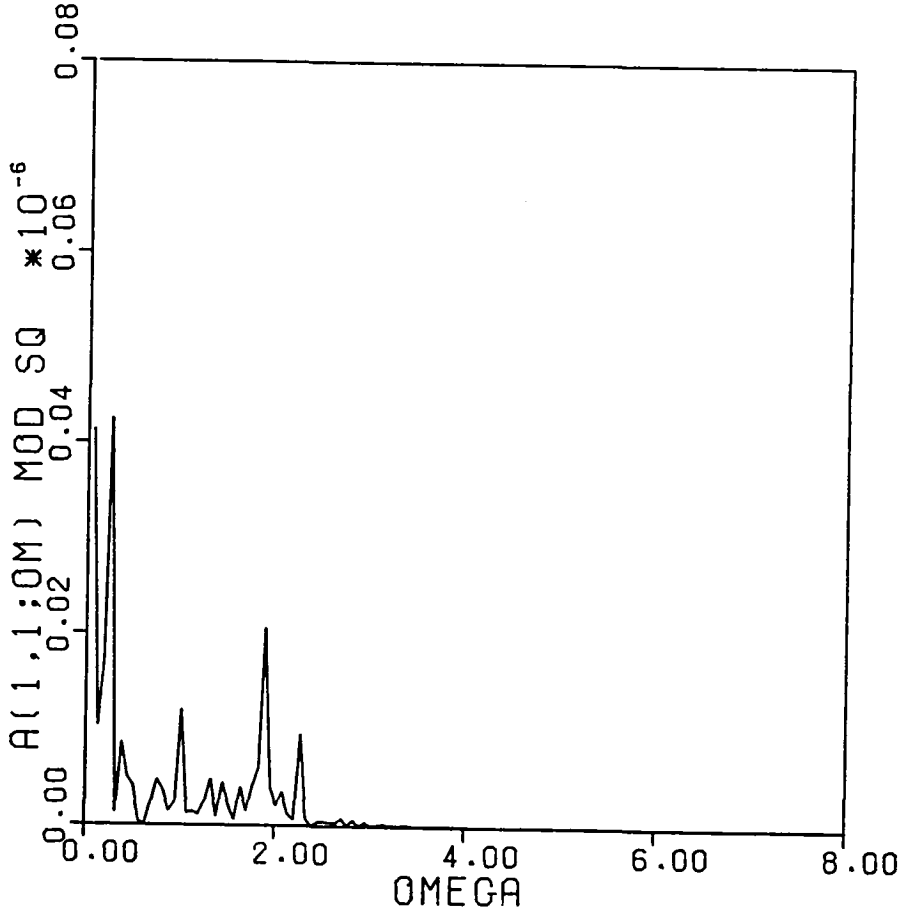

Fig. 6(b)

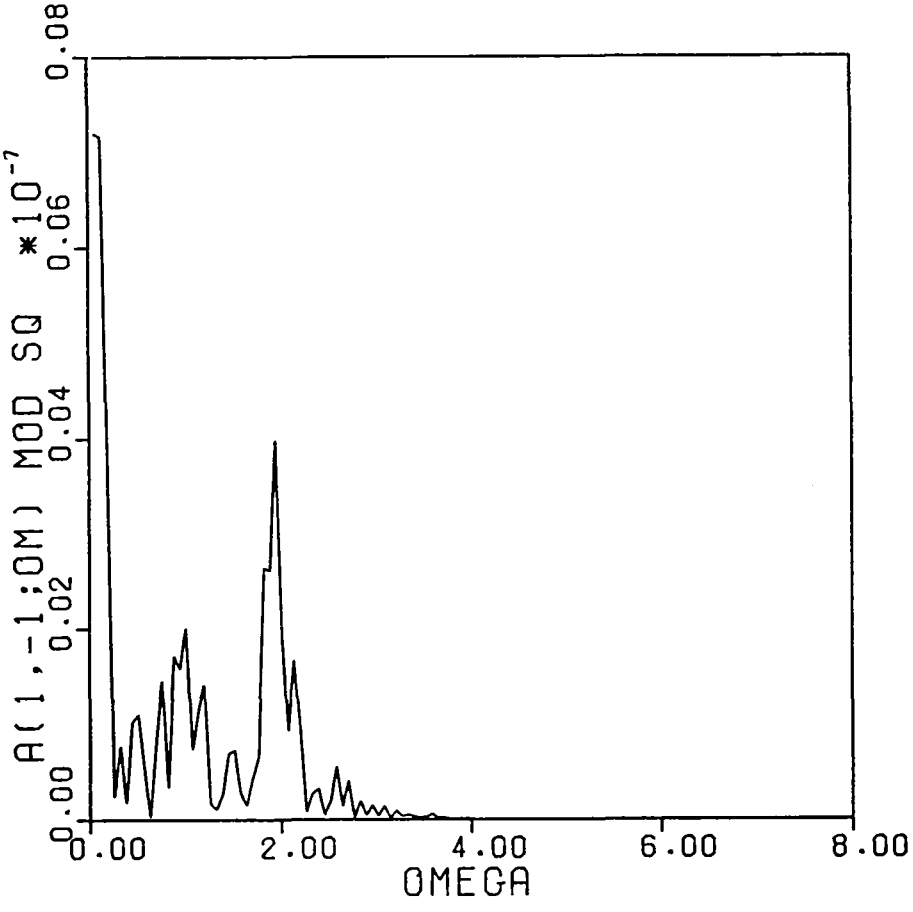

Fig. 6(c)

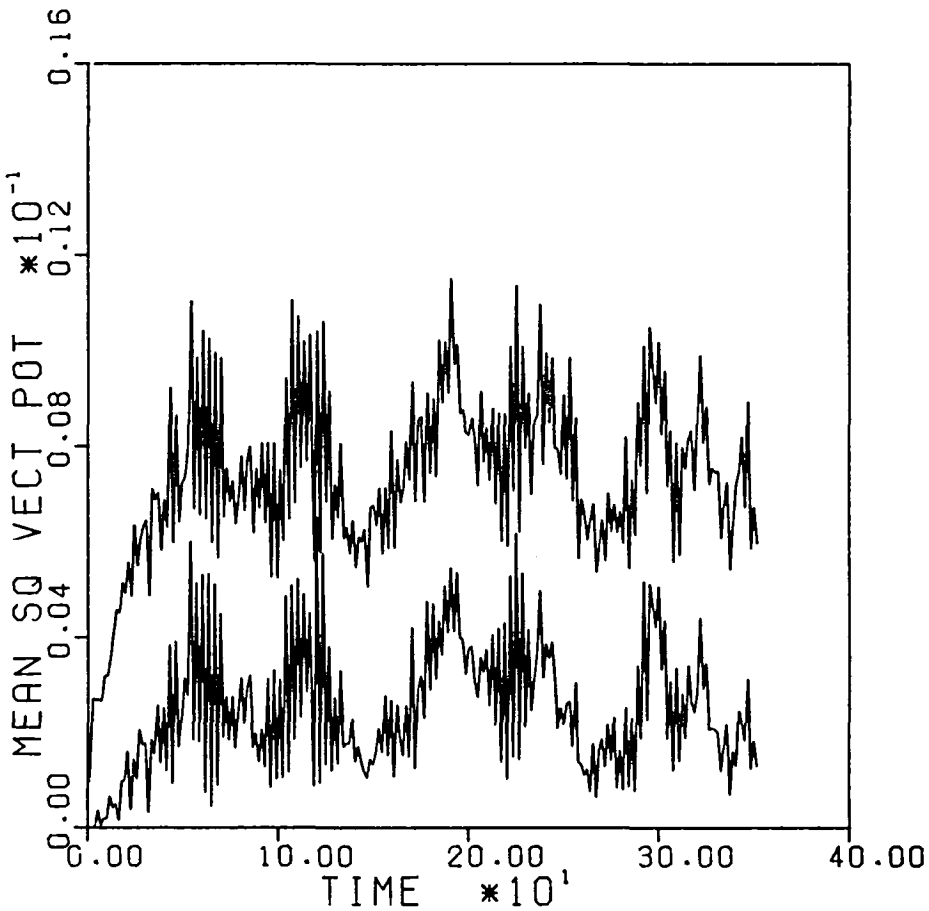
MEAN SQ VECT POT *10⁻¹
0.00
0.04
0.08
0.12
0.16
0.00
10.00
20.00
30.00
40.00
TIME *10¹

Fig. 7

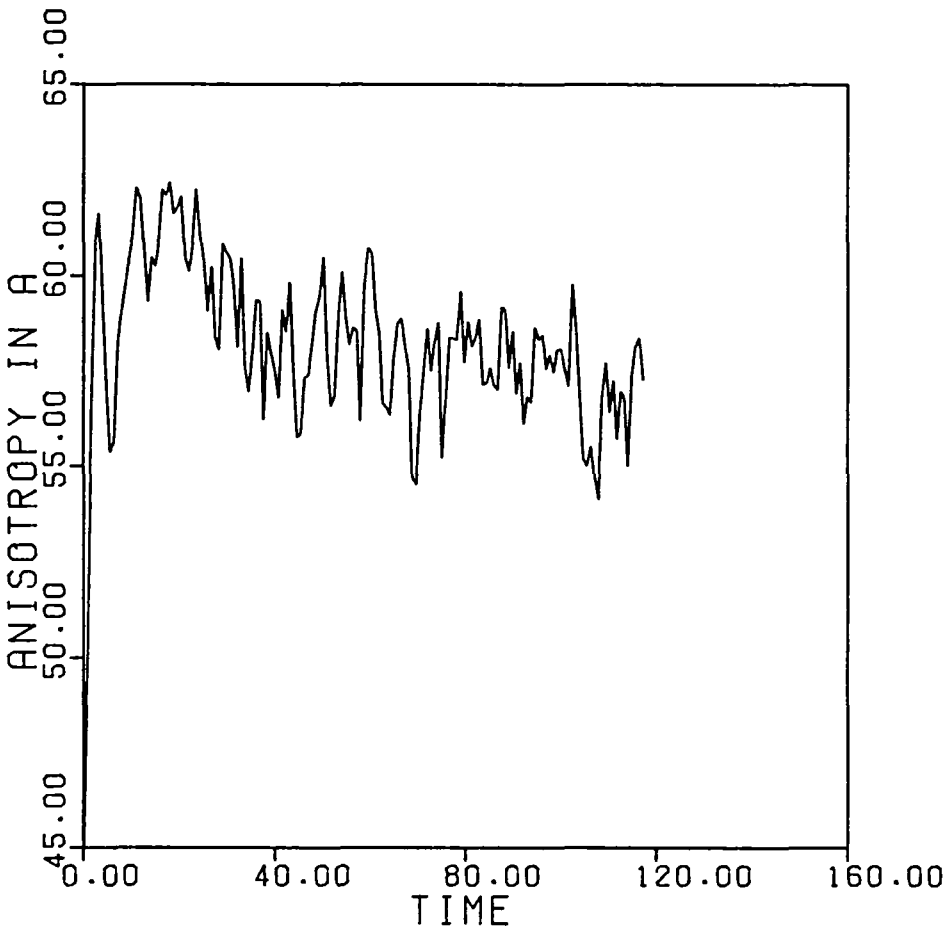
ANISOTROPY IN A
65.00
60.00
55.00
50.00
45.00
0.00
40.00
80.00
120.00
160.00
TIME

Fig. 8(a)

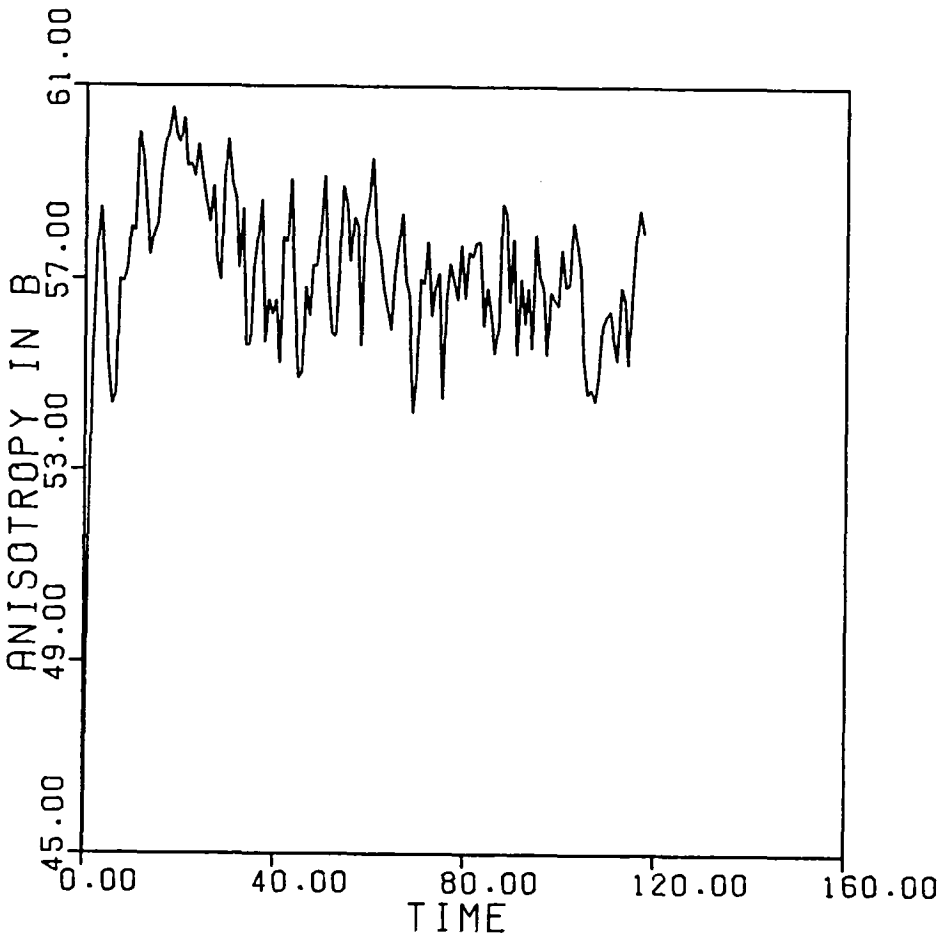
ANISOTROPY IN B
61.00
57.00
53.00
49.00
45.00
0.00
40.00
80.00
120.00
160.00
TIME

Fig. 8(b)

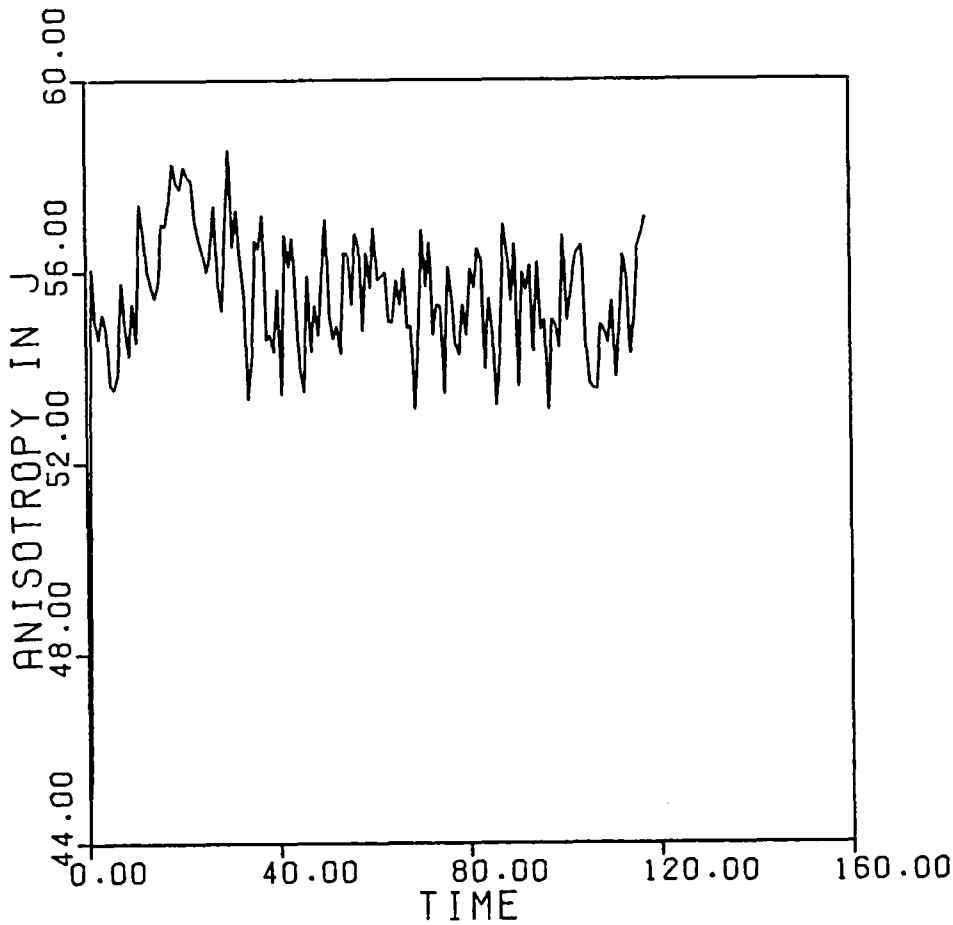
ANISOTROPY IN J
60.00
56.00
52.00
48.00
44.00
0.00
40.00
80.00
120.00
160.00
TIME

Fig. 8(c)

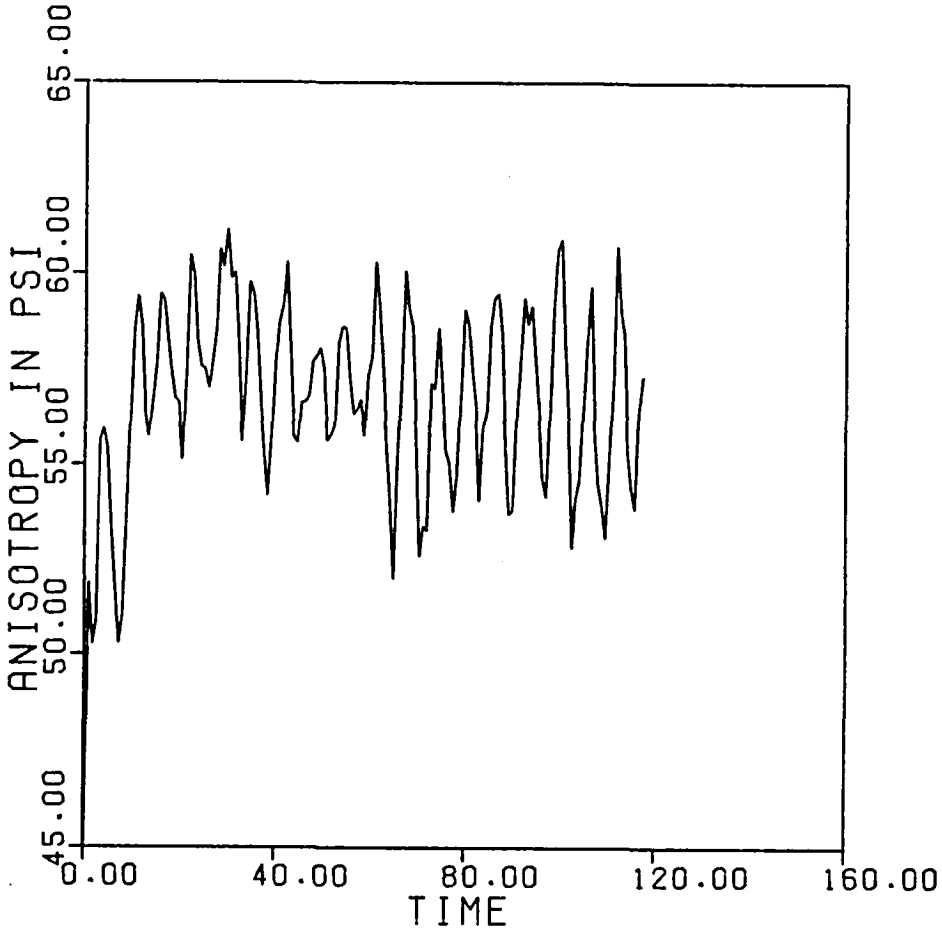
ANISOTROPY IN PSI
65.00
60.00
55.00
50.00
45.00
0.00
40.00
80.00
120.00
160.00
TIME

Fig. 8(d)

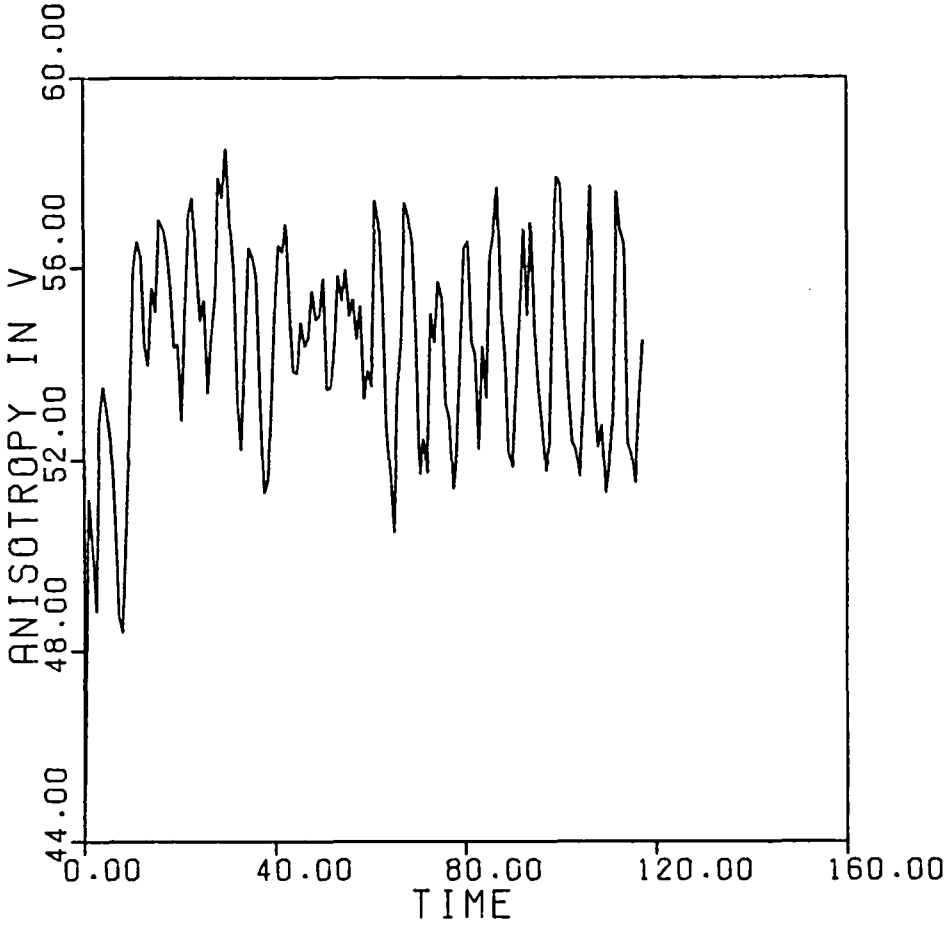
ANISOTROPY IN V
60.00
56.00
52.00
48.00
44.00
0.00
40.00
80.00
120.00
160.00
TIME

Fig. 8(e)

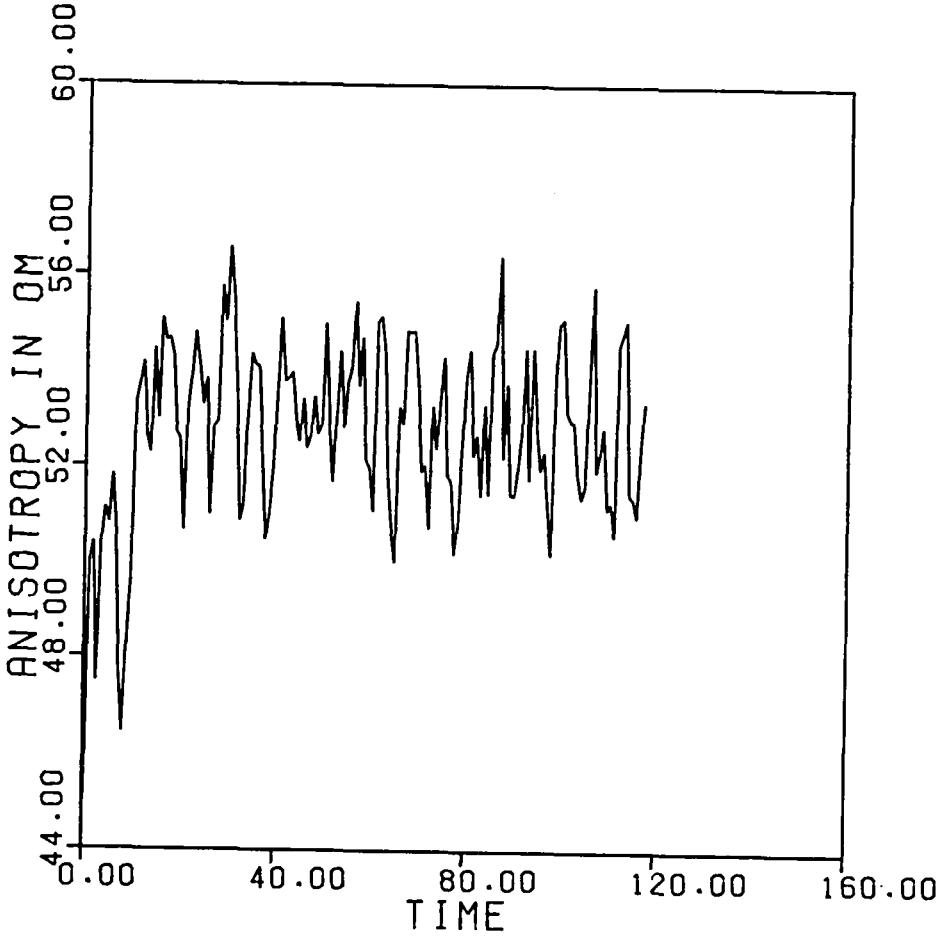
ANISOTROPY IN OM
60.00
56.00
52.00
48.00
44.00
0.00
40.00
80.00
120.00
160.00
TIME

Fig. 8(f)

FIGURE CAPTIONS

Fig. 1(a): Time history of the mean square vector potential for Run A ($B_0 = 0$), which is basically monotonically increasing (upper trace), and for Run C ($B_0 = 0.5$) which exhibits fluctuations after rapid saturation (lower trace). The unit of time is the Alfvén transit time.

Fig. 1(b): Time history of the total energy for Run A ($B_0 = 0$).

Fig. 2(a): Time history of the fluctuating part of the mean square vector potential for Run B ($B_0 = 1.0$).

Fig. 2(b): Time history of the total fluctuating energy for Run B ($B_0 = 1.0$).

Fig. 3(a): Time history of the fluctuating part of the mean square vector potential for Run C ($B_0 = 0.5$). This is the same curve as in Fig. 1(a), but on an expanded scale.

Fig. 3(b): Time history of the total fluctuating energy for Run C ($B_0 = 0.5$).

Fig. 4(a): Contours of constant vector potential for Run A ($B_0 = 0$) at simulation time $t = 234.37$ (time step = 60,000). The dashed contours correspond to negative contour values. Note that like sign contours clumped together.

Fig. 4(b): Contours of constant vector potential for Run B ($B_0 = 1.0$) at $t = 351.56$ (time step = 90,000). Like signs still clumped together but considerably less than that of Fig. 4(a).

Fig. 5(a): Power spectrum of the mean square vector potential for Run A ($B_0 = 0$). The Alfvén frequency is the unit of ω. Frequency components with $\omega \geq 4$ have negligible power spectrum amplitude are not shown.

Fig. 5(b): Power spectrum of the mean square vector potential for Run B ($B_0 = 1.0$), with negligible amplitude for $\omega \geq 8$. Notice a distinct peak at the longest Alfvén frequency $2B_0$.

Fig. 5(c): Power spectrum of the mean square vector potential for Run C ($B_0 = 0.5$). The peak at $\omega = 1$ corresponds to the Alfvén mode with $k_x = 1$.

Fig. 5(d): Power spectrum of the mean square vector potential for Run D ($B_0 = 2.0$). In computing each of these power spectra (Figs. 5(a)-(d)) we have thrown away approximately 12000 initial time steps as transients.

Fig. 6(a): Power spectrum of the Fourier mode $\vec{k} = (1, 0)$ in the mean square vector potential for Run B ($B_0 = 1.0$). Again we see a sharp peak at $\omega = 2B_0$ as in all the power spectra.

Fig. 6(b): Power spectrum of the Fourier mode $\vec{k} = (1, 1)$ in the mean square vector potential for Run B ($B_0 = 1.0$).

Fig. 6(c): Power spectrum of the Fourier mode $\vec{k} = (1, -1)$ in the mean square vector potential for Run B ($B_0 = 1.0$). Only 128 data points are used for computing the power spectra in Figs. 6(a)-(c) while 16384 data points were used for Figs. 5(a)-(d).

Fig. 7: The time development of the mean square vector potential and the contribution of just the sum of the 3 dominating modes $\vec{k} = (1, 0), (1, 1), (1, -1)$. [A(t) plotted here has been coarsed-grained by a factor of 400 over that presented in Fig. 2(a)]. Notice that the coherent nature of the mean square vector potential is due to the above three modes.

Fig. 8: Anisotropy angle, in degrees, as a function of time for Run B ($B_0 = 1.0$) for the fields (a) vector potential a_f, (b) magnetic field $\vec{B}$, (c) current density $\vec{J}$, and (d) stream function ψ, (e) velocity $\vec{v}$, (f) vorticity $\vec{\omega}$. Since (a), (b), (c) is a sequence of increasing k-moments of a_f, we conclude that the anisotropy resides in the long wavelength scales. [Similarly for (d), (e), (f) sequence.]

1. Report No. NASA CR-172576 ICASE Report No. 85-24	2. Government Accession No.	3. Recipient's Catalog No.
4. Title and Subtitle FORCED MHD TURBULENCE IN A UNIFORM EXTERNAL MAGNETIC FIELD		5. Report Date March 1985 6. Performing Organization Code
7. Author(s) Murshed Hossain, George Vahala, David Montgomery		8. Performing Organization Report No. 85-24 10. Work Unit No.
9. Performing Organization Name and Address Institute for Computer Applications in Science and Engineering Mail Stop 132C, NASA Langley Research Center Hampton, VA 23665		11. Contract or Grant No. NAS1-17070 13. Type of Report and Period Covered Contractor Report
12. Sponsoring Agency Name and Address National Aeronautics and Space Administration Washington, D.C. 20546		14. Sponsoring Agency Code 505-31-83-01
15. Supplementary Notes Langley Technical Monitor: J. C. South, Jr. Final Report Additional Support: U.S.D.O.E. Grant Nos. DE-FG05-84ER53176 & DE-FG02-85ER53194 and NASA Grant NAGW-710.		Submitted to Physics of Fluids

16. Abstract

Two-dimensional dissipative MHD turbulence is randomly driven at small spatial scales and is studied by numerical simulation in the presence of a strong uniform external magnetic field. A novel behavior is observed which is apparently distinct from the inverse cascade which prevails in the absence of an external magnetic field. The magnetic spectrum becomes dominated by the three longest-wavelength Alfvén waves in the system allowed by the boundary conditions: those which, in a box size of edge 2π, have wave numbers $(k_x, k_y) = (1, 0)$, $(1, 1)$, and $(1, -1)$, where the external magnetic field is in the x direction. At any given instant, one of these three modes dominates the vector potential spectrum, but they do not constitute a resonantly coupled triad. Rather, they are apparently coupled by the smaller-scale turbulence.

17. Key Words (Suggested by Author(s)) MHD turbulence forced dissipative MHD Alfvén waves and turbulence	18. Distribution Statement 75 - Plasma Physics Unclassified - Unlimited		
19. Security Classif. (of this report) Unclassified	20. Security Classif. (of this page) Unclassified	21. No. of Pages 40	22. Price A03

For sale by the National Technical Information Service, Springfield, Virginia 22161 NASA-Langley, 1985